Journal of Catalysis 259 (2008) 111–122

Contents lists available at ScienceDirect

Journal of Catalysis

www.elsevier.com/locate/jcat

Hydrodechlorination of 1,2-dichloroethane catalyzed by dendrimer-derived Pt–Cu/SiO_2 catalysts

Hong Xie [a,1], Jane Y. Howe [b], Viviane Schwartz [c], John R. Monnier [a], Christopher T. Williams [a,*], Harry J. Ploehn [a]

[a] Department of Chemical Engineering, University of South Carolina, Columbia, SC 29208, USA
[b] HTML, Oak Ridge National Laboratory, Oak Ridge, TN 37831, USA
[c] CNMS, Oak Ridge National Laboratory, Oak Ridge, TN 37831, USA

ARTICLE INFO

Article history:
Received 3 March 2008
Revised 30 July 2008
Accepted 31 July 2008
Available online 30 August 2008

Keywords:
Platinum
Copper
Bimetallic
Dichloroethane
Dendrimer

ABSTRACT

Dendrimer-metal-nanocomposites (DMNs) were used as precursors to prepare SiO_2-supported monometallic Pt, Cu, and bimetallic Pt–Cu catalysts with Pt/Cu atomic ratios of 1:1 ($Pt_{50}Cu_{50}$) and 1:3 ($Pt_{25}Cu_{75}$). After impregnation of these DMNs onto the support, the catalysts were thermally treated and activated following an optimized protocol. Scanning transmission electron microscopy (STEM) showed that the metal nanoparticles in the dendrimer-derived SiO_2-supported catalysts were smaller and had a narrower size distribution compared with those in conventional catalysts prepared using corresponding metal salts via the wet-impregnation method. Slow deactivation was observed for hydrodechlorination of 1,2-dichloroethane over monometallic Cu catalysts, which showed an activity about one to two orders of magnitude lower than that of the Pt-containing catalysts. Hydrodechlorination of 1,2-dichloroethane over the Pt and $Pt_{50}Cu_{50}$ catalysts produced mainly ethane, and the selectivity toward ethane increased with temperature. For the $Pt_{25}Cu_{75}$ catalyst, the selectivity toward ethane decreased in favor of that of ethylene. The overall activity decreased with increasing Cu loading in the catalysts. Activity based on surface Pt sites suggests the formation of bifunctional surfaces in $Pt_{25}Cu_{75}$ catalyst favoring C–Cl bond scission on Cu sites and hydrogenation of intermediate $\cdot CH_2CH_2\cdot$ on Pt sites. In addition, kinetic analyses suggest different reaction mechanisms for hydrodechlorination of 1,2-dichloroethane over Pt and Cu-enriched surfaces in the Pt–Cu bimetallic catalysts.

1. Introduction

Chlorinated hydrocarbon byproducts from many industrial processes are serious environmental pollutants. Technologies to eliminate these chlorinated compounds from industrial waste streams have been actively sought [1,2]. Whereas Group VIII metal-based monometallic Pt or Pd catalysts are effective for hydrodechlorination, they do not fully convert di-chlorinated hydrocarbons into nonchlorinated hydrocarbons. In addition, during the conversion of dichloroethane, the intermediate ethylene product is readily converted into ethane, which is much less useful from an economic standpoint [3,4]. In contrast, group IB-based monometallic Cu or Sn catalysts are effective for full dechlorination of chlorinated hydrocarbons with higher selectivity toward ethylene; however, such catalysts are less active under mild conditions and can be further deactivated at relatively high temperature after a long time on stream.

It has long been known that bimetallic surfaces can exhibit chemical and catalytic properties that differ greatly from those of the individual metals [5,6]. In recent years, there has been a considerable increase in research into bimetallic catalysts that can improve the reaction selectivity and stability toward selective products [7–13]. Whereas an electronic (i.e., ligand) effect would be expected to influence both the selectivity and activity of bimetallic catalysts [14], previous work [5] has indicated that ensemble and/or geometric effects at the surface may play a crucial role in determining the selectivity. Many compounds of Group IB metals have been used as modifiers of active metals of Group VIII [11]; for example, Pt- and Pd-containing bimetallic catalysts can be formed by adding a secondary metal, such as Cu, Ag, or Sn [4,5,11,15]. Selective dechlorination of chlorinated alkanes into dechlorinated alkenes has been investigated by several groups using different bimetallic catalysts, including Pt–Cu by d'Itri et al. [16–18], Pd–Ag by Heinrichs et al. [4,19–22], Pd–Pt by Karpinski et al. [23], and Pt–Sn bimetallic catalysts [4,15]. Preparation of such bimetallic catalysts has also been proposed in patents from Dow Chemical [24] using an active hydrogenating metal of Pt/Ir and a surface segregating metal of Cu, and from Solvay by Heinrichs et al. [25] using Pd and Ag.

* Corresponding author. Fax: +1 803 777 8265.
E-mail address: willia84@engr.sc.edu (C.T. Williams).
[1] Current affiliation: CNMS, Oak Ridge National Laboratory Oak Ridge, TN 37831, USA.

0021-9517/$ – see front matter
doi:10.1016/j.jcat.2008.07.018

Fundamental research on various aspects of Cu and Pt has been carried out in recent years; for example, CO adsorption on a stepped Cu(332) surface has been studied during adsorption and desorption [26], and CO adsorption on Cu(111) has been examined at low temperatures (25–150 K) by reflection absorption infrared spectroscopy [27]. A systematic study of CO oxidation on the $Cu_3Pt(111)$ alloy surface by means of DFT calculations has shown that the adsorption energy of CO decreases on Pt (or Cu) on the alloy with respect to those on the pure metals. This implies that Cu_3Pt alloy might be a better catalyst for CO oxidation than pure Pt [28]. In electrocatalysis applications, carbon-supported Pt–Cu alloys have been synthesized at temperatures up to 950 °C [29,30]. The synthesis of carbon-supported Cu-rich Pt–Cu alloys involved electrochemical dissolution of Cu. At the end of the dissolution process, the $Pt_{25}Cu_{75}$ precursor alloy changed into a substantially Pt enriched Pt–Cu alloy ($Pt_{79}Cu_{21}$) with an essentially pure Pt surface ($Pt_{93}Cu_7$) [30]. Nanoporous Pt also has been produced through the selective dissolution of Cu from $Pt_{0.75}Cu_{0.25}$ at room temperature [31].

In this work, we explored the effectiveness of using poly(amido amine) (PAMAM) dendrimer metal nanocomposites (DMNs) as precursors for supported bimetallic catalyst synthesis. Dendrimers are a class of monodispersed, highly branched polymers with well-defined three-dimensional architectures [32,33] that can create interior voids to accommodate guest molecules. In 1985, Tomalia et al. [34] published the synthesis and characterization of PAMAM macromolecules and referred to these polymers as dendrimers. These dendrimers feature interior amide and amine groups that can physically coordinate with metal cations or bond covalently with metal precursors through ligand exchange. The branched structure of dendrimers can terminate with various exterior surface groups (e.g., hydroxyl, carboxyl) useful for further functionalization. The number of exterior groups increases as 2^{N+2}, where N is the generation number. For dendrimers of higher generations, the need to pack braches into a limited space results in steric constraints that can possibly limit the accessibility of the metal cations to dendrimer interior groups; therefore, in this work we used a medium generation 4 (G4) dendrimer, to allow accessibility of metal cations to the interior functional groups. Thus, the goal of this work is to relate various structural aspects of the dendrimer-derived bimetallic Pt–Cu/SiO_2 catalysts to their activity and selectivity in the hydrodechlorination of 1,2-dichloroethane.

2. Experimental

2.1. Catalyst preparation

Mesoporous nonacidic SiO_2 support, obtained from BASF Catalysts, had a BET surface area of 67 m^2/g and an average pore diameter of 30 nm. The support was used as received. $H_2PtCl_6 \cdot 6H_2O$ (99.9%) and $CuCl_2$ (99%) were purchased from Alfa. 1,2-Dichloroethane (99.8%) and PAMAM G4OH dendrimer (10 wt% in methanol) were purchased from Aldrich. Before use, the methanol solvent in PAMAM G4OH dendrimer solution was removed by flowing N_2 at room temperature. Water was deionized to a resistivity of 18 MΩ cm using a Nanopure system (Barnstead).

Dendrimer-derived monometallic Pt and bimetallic Pt–Cu nanocomposites with Pt/Cu atomic ratio of 1:1 ($Pt_{50}Cu_{50}$) and 1:3 ($Pt_{25}Cu_{75}$) were synthesized in aqueous PAMAM G4OH dendrimer solutions. The subscripts refer to the atomic ratios of metal atoms per G4OH molecule in solution. The synthesis of monometallic Pt nanocomposites was done as described previously [35–37]. For the bimetallic DMN synthesis, aqueous H_2PtCl_6 and $CuCl_2$ precursor solutions were added simultaneously to the G4OH dendrimer solution. All of the Pt-containing nanocomposites had a nominal metal-to-dendrimer molar ratio of 40:1. These aqueous nanocomposites were kept in the dark and stirred thoroughly for 10 days, to allow completion of the dendrimer–metal ligand-exchange reaction. Supported catalysts were prepared by subsequently depositing these aqueous DMNs onto the silica support through wet impregnation at room temperature. Corresponding conventional catalysts also were prepared by wet impregnation of solutions of the salts, but without the G4OH dendrimer.

After impregnation, all of the supported catalyst samples were dried at room temperature under vigorous stirring in a ventilated hood to remove the residual moisture. All sample powders were ground before further calcination and reduction. Based on our previous dendrimer decomposition studies [38,39], all samples were calcined in 10% O_2 (He balance) at 350 °C for 1 h, to decompose dendrimers and remove the impurities from the support. They were then reduced in flowing H_2 for 1 h at 350 °C to produce the final catalysts. For convenience, we designate the catalysts prepared by DMN as dendrimer-derived (DD) and conventionally derived catalysts as CD.

Different metal loadings were obtained for all catalysts by adjusting the concentrations of the precursors and the amount of the SiO_2 support used in the impregnating solutions. All of the Pt-containing catalysts had approximately 2 wt% Pt. The weight loadings were 2% for Pt/SiO_2, 2% Pt + 0.65% Cu for $Pt_{50}Cu_{50}/SiO_2$, 2% Pt + 1.95% Cu for $Pt_{25}Cu_{75}/SiO_2$, and 1% for Cu/SiO_2. The metal loadings in this study were confirmed by elemental analysis via atomic adsorption spectroscopy and are accurate to within ±5%.

2.2. Catalyst characterization

Scanning transmission electron microscopy (STEM) measurements were carried out on a Hitachi HD2000 instrument at Oak Ridge National Laboratory, operating at 200 kV under HAADF Z-contrast mode with a resolution of 0.24 nm. Ground catalyst fine powders were supported on holey carbon film-coated nickel grids. Histograms of particle size were obtained after measurement of more than 200 randomly selected particles from at least 5 images for each sample. The experimental volume-surface mean diameters (VSMD) of the particles in different samples were calculated using the following equation:

$$\bar{D} = \frac{\sum_1^N D_i^3}{\sum_1^N D_i^2},$$

where D_i is the diameter of each nanoparticle. The VSMD is an indicator of the particle diameter in which most of the metal atoms reside.

In situ Fourier transform infrared (FTIR) spectra were recorded using a Nicolet 4700 spectrometer equipped with a liquid N_2-cooled MCT/A detector. Carbon monoxide adsorption spectra were collected at room temperature in the single-beam transmission mode with a resolution of 2 cm^{-1} and 64 scans accumulated per spectrum. Catalyst samples were prepared as 15 mg/cm^2 self-supporting wafers with a diameter of 12 mm by pressing the preground powder of supported metal precursors at 10,000 lb for 1 min. The wafers were then placed into a sample holder inside a homemade gas flow IR transmission cell with a 10-cm light path length. The IR cell was made of stainless steel with NaCl crystal windows on both ends cooled by flowing water. The cell was equipped with stainless steel gas inlet outlet ports and a thermocouple port. A heating cord (Glass-Col 103B SCC4) was wrapped around the cell for thermal treatment. The temperature was monitored via a K-type thermocouple in close proximity with the catalyst pellet and controlled with a temperature controller (Omega CN2011). The total gas flow rate was maintained at 70 cm^3/min. The catalysts were calcined and reduced as described above, and then cooled to room temperature in H_2. CO adsorption experiments were conducted at this point. Background references were

first recorded after the flow cell was purged for 10 min with He before flowing 1% CO (He balance) for 15 min. This was followed by a second purge of He for a specified period, during which the spectra of adsorbed CO were collected every 5 min.

H_2 chemisorption was used to measure the Pt dispersion in Pt-containing catalysts using a Micromeritics 2750 instrument with a pulse chemisorption mode. The calcined catalyst sample (0.2–0.4 g) was placed into a glass U-tube reactor and reduced in flowing H_2 at 350 °C for 1 h before being cooled to 40 °C for measurement. Argon was used as the carrying gas, and the total flow rate was fixed at 20 cm^3/min. H_2 loop gas (0.101 cm^3) was used for each pulse, and at least 4 pulses were introduced to guarantee that no further H_2 could be adsorbed on the catalyst. The amount of H_2 was monitored using a thermal conductivity detector.

2.3. Catalyst evaluation

Hydrodechlorination of 1,2-dichloroethane (DCE) was carried out under atmospheric pressure in a tubular Pyrex microreactor (10 mm), inside which 0.1 g of catalyst was supported on a fritted disk. A constant flow of each gas stream was metered using Tylan FC-260 mass flow controllers and mixed as necessary before it entered the reactor. The DCE was metered into the reaction system by flowing a sweep gas of He through a VLE saturator filled with the liquid DCE. A constant DCE concentration was ensured by maintaining the saturator at a fixed temperature of 9.0 ± 0.2 °C using a recirculation cooling system and a constant sweep gas flow rate. A thermocouple embedded in the catalyst bed was used to monitor the catalyst temperature. The catalyst temperature was maintained at the desired temperature ±0.5 °C using an electric furnace heating system.

Before reaction, each catalyst was pretreated *in situ* in flowing 10% O_2 (He balance) to decompose the dendrimers and/or remove impurities. The temperature was ramped up from 25 to 350 °C at 5.4 °C/min and held at 350 °C for 1 h before the flowing gas was switched to H_2 for reduction at the same temperature of 350 °C for 1 h. The temperature of the catalyst was then lowered to the reaction temperature in H_2 and held there for 20 min before the reactants were introduced to the catalyst. The total gas flow rate for calcination and reduction was fixed at 200 sccm. The feed composition for the reaction was 1.6% DCE, 16.4% H_2, and balance He. The total flow rate of the feed was 61 sccm, for a GHSV of 14,900 h^{-1}. The effluents were analyzed by gas chromatography (HP 5890 series II with a flame ionization detector) using a 30-m-long Poraplot Q capillary column. Gas samples were injected into the gas chromatograph at specified time intervals from 10 min to 2 h after the required temperature was attained. Calculation of the mass balance for the conversion of DCE and the product selectivity was based on a carbon balance and was confirmed to within 5% by quantitative analysis of reactants and products. Catalyst deactivation studies also were carried out with time on stream (TOS) up to 30 h.

3. Results and discussion

3.1. STEM analysis

STEM images of the reduced Pt-containing catalysts (Fig. 1) indicate a roughly spherical Pt particle morphology in all cases. Particle sizes and distributions differed between the DD catalysts and their CD counterparts (Fig. 2); in general, smaller particle sizes with narrower size distribution were obtained for the DD cata-

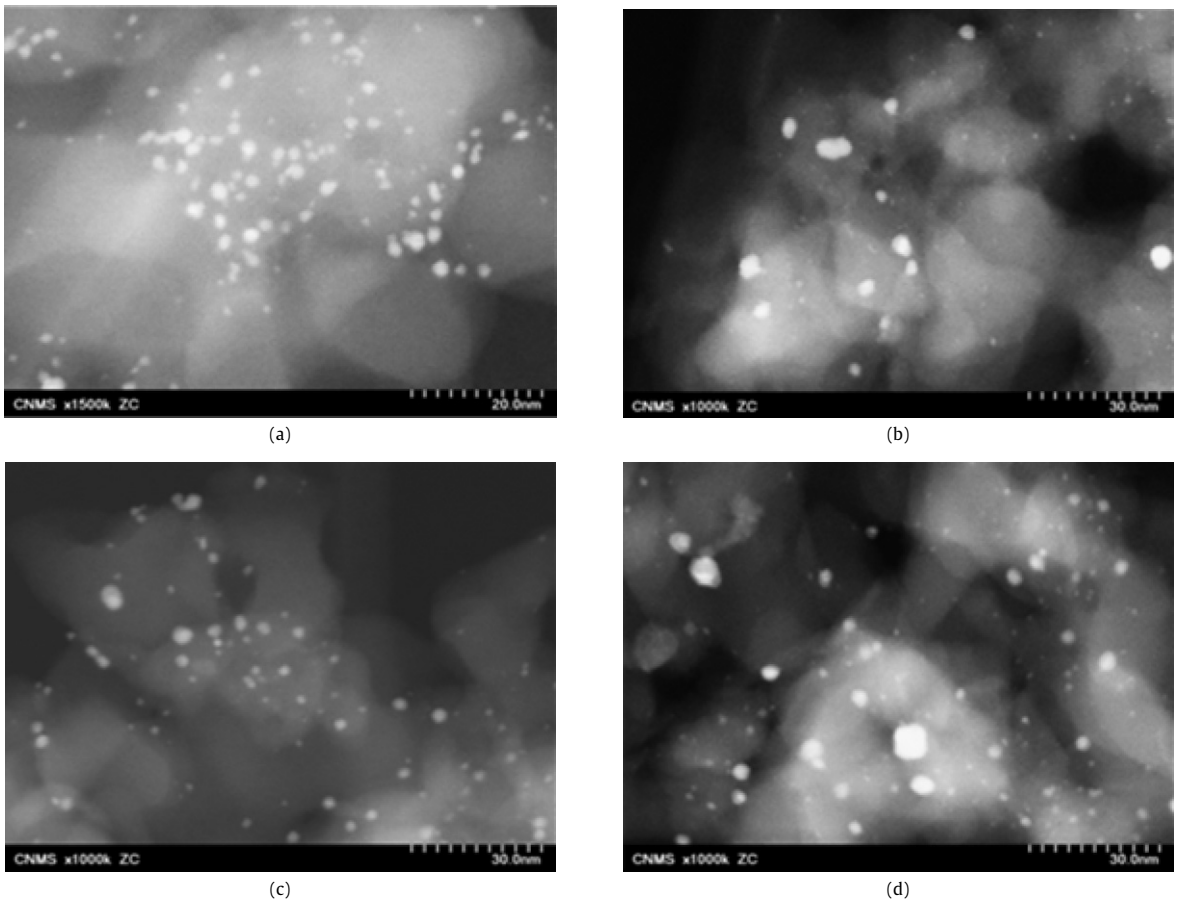

Fig. 1. STEM images of DD and CD catalysts (a) Pt-DD, (b) Pt-CD, (c) $Pt_{50}Cu_{50}$-DD, (d) $Pt_{50}Cu_{50}$-CD, (e) $Pt_{25}Cu_{75}$-DD, and (f) $Pt_{25}Cu_{75}$-CD.

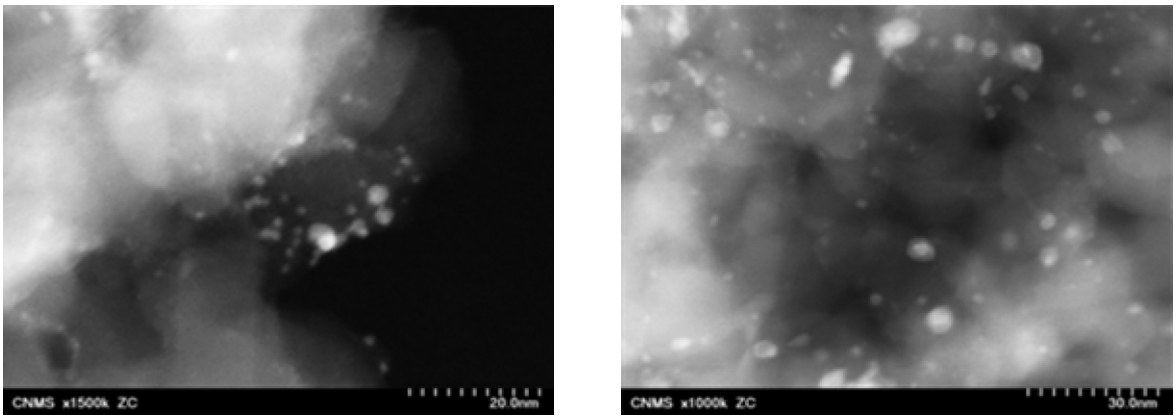

(e) (f)

Fig. 1. (*continued*)

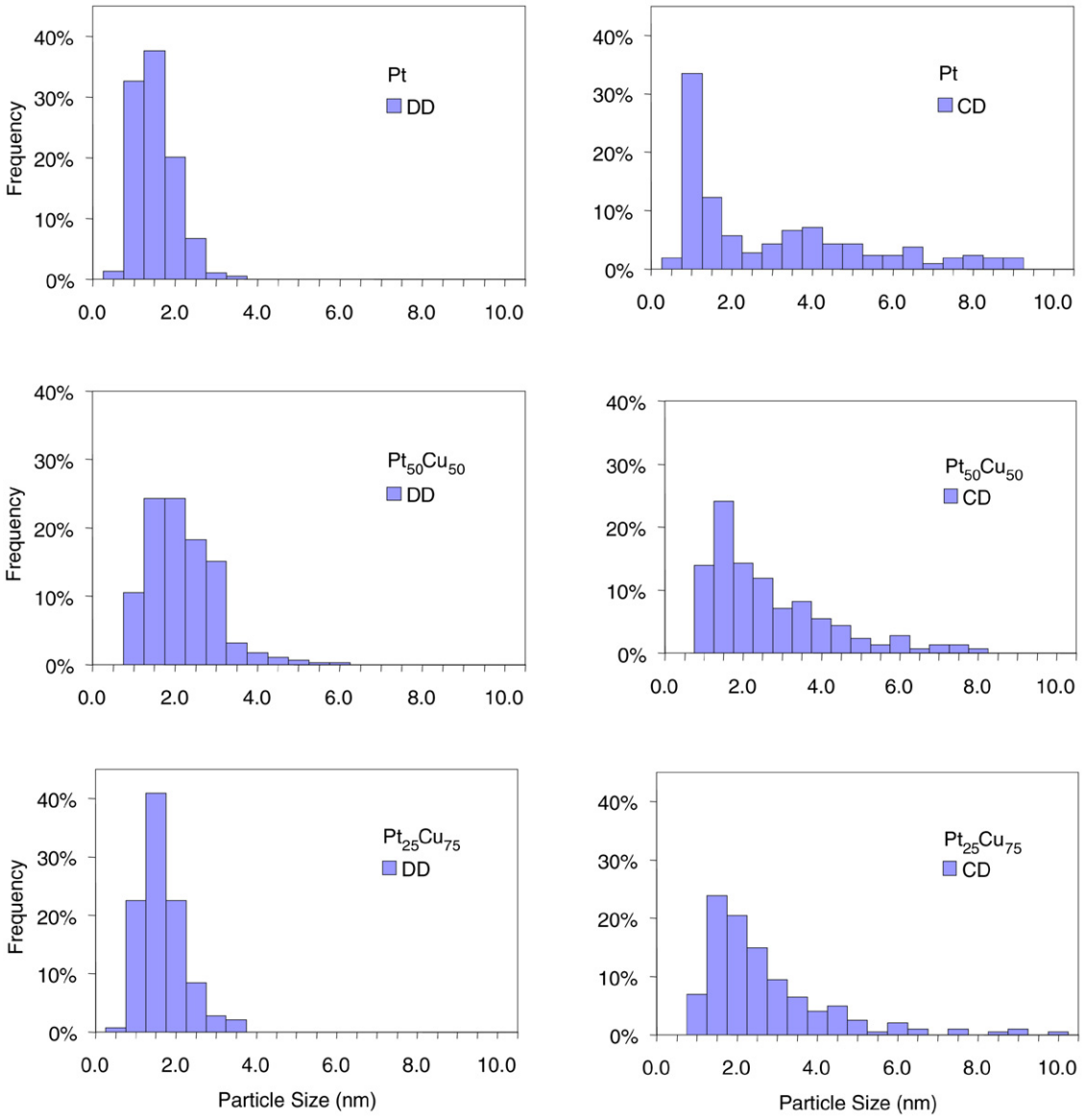

Fig. 2. Size distributions of the supported catalysts after calcination and reduction.

lysts. As shown in Table 1, calculation of VSMD shows that the metal in the DD catalysts resided in smaller-diameter nanoparticles on average; thus, the G4OH dendrimer exerted significant control over particle formation and sintering on the catalyst support. Given this more precise control over structure in the DD catalysts, we focused our FTIR and kinetic studies on these materials. Further

Table 1
Mean size and volume surface mean diameter (VSMD) for Pt and Pt–Cu catalysts

	Pt		$Pt_{50}Cu_{50}$		$Pt_{25}Cu_{75}$	
	DD	CD	DD	CD	DD	CD
Mean size (nm)	1.5 ± 0.5	3.0 ± 2.3	2.2 ± 0.8	2.6 ± 1.6	1.6 ± 0.6	2.7 ± 1.6
VSMD (nm)	1.4	6.1	2.8	4.4	2.1	4.9

X-ray diffraction measurements showed that the two DD bimetallic catalysts are composed of a mixture phase of Pt and Cu and a Pt–Cu alloy phase (see supplementary information).

3.2. FTIR spectroscopy of adsorbed CO

IR spectra of CO absorption on the DD catalysts were measured at room temperature to explore the effect of Cu on the surface structure and electronic properties of Pt ensembles. Experiments were performed on both reduced and reoxidized DD catalysts. The reduced catalysts were treated based on the aforementioned standard treatment protocol. To prepare the reoxidized catalysts, after reduction in H_2 at 350 °C, an additional 1 h of treatment in 10% O_2 (He balance) was provided, followed by cooling.

3.2.1. CO adsorption on reduced and oxidized Pt-containing catalysts

Figs. 3 and 4 show FTIR spectra of adsorbed CO on reduced and reoxidized DD catalysts, respectively. Table 2 summarizes the band frequencies of the different features shown in the figures. For the reduced catalysts, each spectrum shows a main band with peak positions ranging from 2072 to 2058 cm^{-1} depending on the Cu loading, corresponding to linearly bonded CO on Pt [40,41]. These bands exhibit low-frequency inhomogeneous line broadening, as has been found in CO adsorption spectra between 2070 and 2020 cm^{-1} [40,41]. This line-broadening arises from the presence of more than one linear CO adsorption mode [41,42]. For

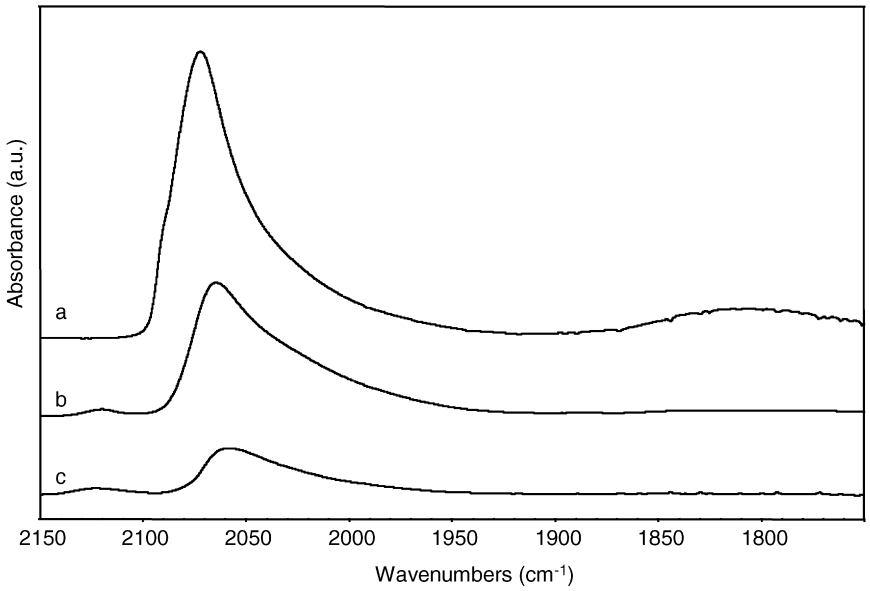

Fig. 3. FTIR spectra of CO adsorption on reduced Pt-containing catalysts after saturation of the surface with CO followed by purging He for 15 min at room temperature: (a) Pt, (b) $Pt_{50}Cu_{50}$, and (c) $Pt_{25}Cu_{75}$.

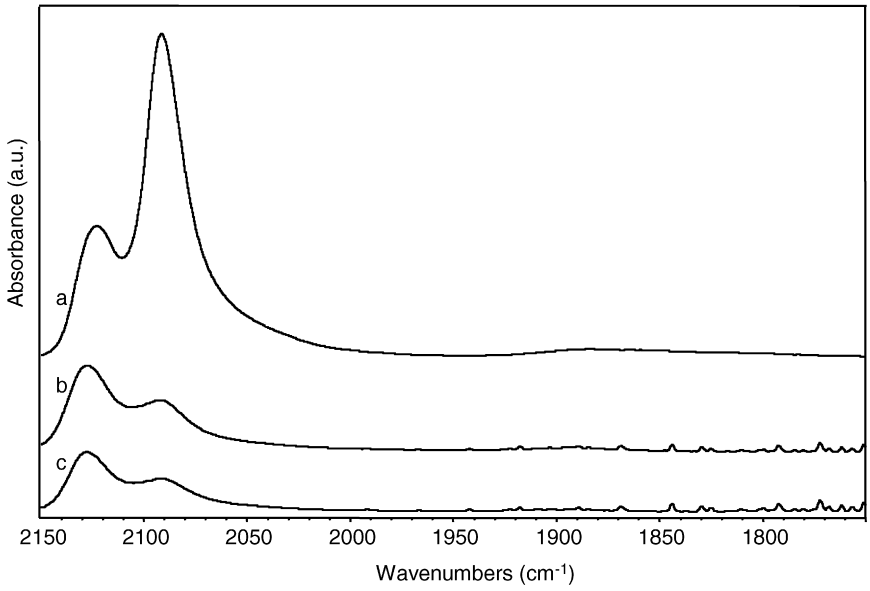

Fig. 4. FTIR spectra of CO adsorption on re-oxidized Pt-containing catalysts after saturation of the surface with CO followed by purging He for 15 min at room temperature: (a) Pt, (b) $Pt_{50}Cu_{50}$, and (c) $Pt_{25}Cu_{75}$.

Table 2
Summary of CO adsorption band frequency (cm^{-1}) for reduced and oxidized catalysts

Catalysts	Pt	$Pt_{50}Cu_{50}$	$Pt_{25}Cu_{75}$	Band assignment	Reference
Reduced		2120	2123	$Cu^{\delta+}$ $(0<\delta<2)$	[47,49,50]
	2090[a]			Pt^{n+} $(\delta<n<1)$	[48]
	2072	2065	2058	Linear CO on Pt(111)	[40,41]
	1805			3-fold bridged CO	[41,45,46]
Re-Oxidized		2127	2128	$Cu^{\delta+}$ $(0<\delta<2)$	[47,49,50]
	2123			Pt^{m+} $(1<m<2)$	[48]
	2092	2092	2091	Pt^{n+} $(\delta<n<1)$	[48]
	1885			2-fold bridged CO	[41]

[a] This band is visible as a shoulder.

the monometallic Pt catalyst, a distinct high-frequency shoulder at ca. 2090 cm^{-1} also was observed along with the low-frequency inhomogeneous line-broadening. Bands of similar shape at high, medium, and low frequencies have been interpreted as CO adsorbed on different crystallite facet faces, corners, and edges, respectively [42–44]. Moreover, 3-fold bridged CO is evident from the broad peak centered at 1805 cm^{-1} [41,45,46].

With the addition of Cu, the main band on Pt shifted from 2072 cm^{-1} to 2068 cm^{-1} for the $Pt_{50}Cu_{50}$ catalyst and to 2058 cm^{-1} for the $Pt_{25}Cu_{75}$ catalyst. This observation may be explained by the dilution of Pt ensembles with Cu. The addition of Cu may lead to a greater electron density on surface Pt, which allows for increased back-donation of electrons to CO π^* orbitals [47]. Alternatively, the addition of Cu to Pt also may result in the formation of a different intraparticle morphology. In this case, the addition of Cu may cover the terraces of Pt crystallites, thereby decreasing the available higher-coordination Pt sites and lowering the CO vibrational frequency. The XRD measurements of these Pt-containing catalysts (see supplementary information) yield further insights for interpreting these CO spectra. For the $Pt_{50}Cu_{50}$ catalyst, the XRD results suggest that two separate phases of Pt and Pt–Cu alloy were formed, with the Pt phase dominating. Thus, formation of the Pt–Cu alloy contributes to the slight (4 cm^{-1}) blue shift of the main CO adsorption band from 2072 cm^{-1} for Pt to 2068 cm^{-1} for $Pt_{50}Cu_{50}$. For the $Pt_{25}Cu_{75}$ catalyst, the XRD results show that a more pronounced Pt–Cu alloy phase was formed compared with that of the $Pt_{50}Cu_{50}$ catalyst, as confirmed by a new peak centered at $2\theta = 41.91°$ (see supplementary information). This can partially account for the 14 cm^{-1} blue shift of the main CO adsorption band from 2072 cm^{-1} to 2058 cm^{-1} for $Pt_{25}Cu_{75}$, although a decrease on dipole coupling may also be occurring (see below). It is also likely that the Cu is breaking the Pt ensembles (or perhaps covering the Pt surface), based on the disappearance of the bridged CO species for the two Pt–Cu catalysts (Fig. 3).

Significant differences in band position for adsorbed CO on Pt were observed for the reoxidized catalysts compared with their reduced counterparts (Fig. 4). Regardless of the Cu loading, all of the bimetallic catalysts exhibited higher-frequency bands at ca. 2130 cm^{-1} and 2090 cm^{-1}. By analogy with the band assignments for CO on Pt/γ-Al_2O_3 [48], this sharp peak at 2090 cm^{-1} can be assigned to partially oxidized Pt^{n+} species $(\delta < n < 1)$. For the oxidized monometallic Pt catalyst, the new band at ca. 2123 cm^{-1} can be assigned to the Pt^{m+} $(1 < m < 2)$ species. In addition, a band at 1885 cm^{-1} due to bridge-bonded CO and a band at ca. 2135 cm^{-1} due to oxidized Cu were seen.

Both reduced bimetallic catalysts exhibited a higher-frequency band at ca. 2121 cm^{-1}, which blue-shifted by ca. 6 cm^{-1} for the reoxidized catalysts. Considering the contributions from two different types of adsorbed CO on catalysts before and after reoxidation is reasonable. The band at ca. 2121 cm^{-1} on the reduced catalysts is associated with Cu species ranging from Cu^0 to Cu^{2+} [47,49,50]; however, in the oxidized catalysts, this feature more likely arises via a combination of both oxidized Cu and Pt^{m+} $(1 < m < 2)$ species [48].

3.2.2. $^{13}CO/^{12}CO$ isotope dilution study

It is clear from Figs. 3 and 4 that the adsorbed CO band frequencies differ considerably between Pt catalysts and Pt–Cu catalysts. Three factors cause such band shifts on supported catalysts and single crystals [51]: (1) dipole–dipole coupling, (2) altered electron transfer between the metal surface and CO, and (3) inherent heterogeneities of the surfaces in supported catalysts. Dipole–dipole coupling causes a band shift due to the interaction between the adjacent dipoles vibrating at roughly the same frequency on the metal surfaces. The band shift due to the dipole coupling occurs when the frequencies of the interacting dipoles are nearly identical. The chemical shift results from the changes in electron distribution between the adsorbed CO and the metal and can be either positive or negative. Surface heterogeneity may complicate the measurement of dipole shift due to the existence of intensity redistribution, which causes the higher-frequency band to effectively mask the lower-frequency band [40,42,52].

Isotope dilution experiments can be used to separate the dipole shift from the chemical shift and other contributions to the stretching frequency of molecules adsorbed on metal surfaces. Essentially, a series of isotopic mixtures of varying composition is dosed onto supported metal surfaces at a given total coverage close to saturation, after which the IR stretching frequency of the adsorbed CO isotope is measured as a function of its concentration. Because ^{12}CO and ^{13}CO have different vibration frequencies, dilution of one in the other will weaken the dipole–dipole coupling interactions. But the chemical shift is a function of the bonding properties of the metal substrate and thus is independent of isotopic substitution in the adlayer. Along these lines, $^{12}CO/^{13}CO$ isotope mixture adsorption experiments were carried out on reduced Pt and $Pt_{25}Cu_{75}$ DD catalysts at room temperature. The total flow rate of CO isotopes was kept at 0.7 cm^3/min with a partial pressure of 7.6 Torr. The volume percentage (concentration) of ^{13}CO was varied from 0% to 100%. FTIR spectra were recorded for each isotope mixture, as shown in Figs. 5 and 6.

For the monometallic Pt-DD catalyst, as the fraction of ^{12}CO for ^{13}CO was varied, the pronounced band for linear ^{12}CO shifted from 2072 (100% ^{12}CO) to 2045 cm^{-1} (13% ^{12}CO) as shown in Fig. 5. On the other hand, when ^{13}CO was <50%, the band for linear ^{13}CO adsorbed on Pt was observed only as a shoulder on the lower side of the intense band (between 2057 and 2072 cm^{-1}) associated with the adsorbed ^{12}CO on Pt. When the ^{13}CO concentration was 75%, the spectrum consisted of two vibrational bands centered at 2047 cm^{-1} for ^{12}CO and 2015 cm^{-1} for ^{13}CO. Exposure to 100% ^{13}CO resulted in a band at 2023 cm^{-1}. For the $Pt_{25}Cu_{75}$-DD catalyst (Fig. 6), no obvious band shift in the ^{12}CO frequency was observed from 100% ^{12}CO to 78% ^{12}CO. Indeed, d'Itri et al. [33] reported that the position of the ^{12}CO band on Pt on low metal loading Pt–Cu catalysts with the Pt/Cu atomic ratio of 0.3 was independent of the ^{12}CO concentration during isotopic dilution experiments; however, in the present case, the linear ^{12}CO band clearly shifted from 2059 (78% ^{12}CO) to 2045 cm^{-1} (13% ^{12}CO) as the amount of ^{12}CO was decreased (Fig. 6).

Fig. 7 plots the frequency of ^{12}CO on both catalysts as a function of the ^{12}CO concentration in the isotope mixture. Extrapolating to infinite dilution of ^{12}CO in ^{13}CO, the intercept can be interpreted as the peak position of ^{12}CO in the absence of dipole coupling. This frequency is the dipole singleton frequency for ^{12}CO on Pt [42]. The dipole shift is calculated by subtracting this dipole singleton frequency from the frequency obtained at 100% ^{12}CO. In the case of the Pt-DD catalyst, a linear curve fit of the data (triangles) shows a ^{12}CO singleton frequency of 2040 ± 2 cm^{-1}. This indicates a dipole shift of around 32 cm^{-1} and is consistent in magnitude

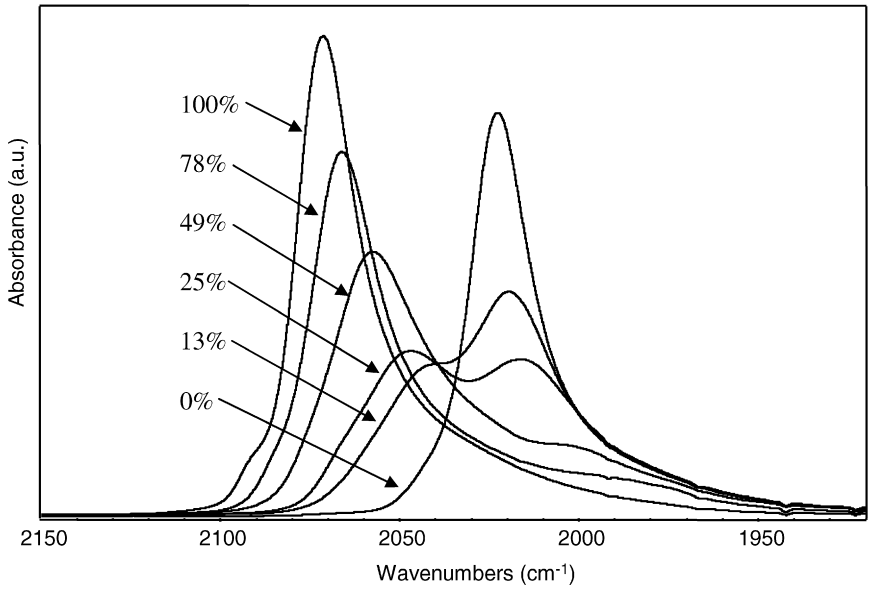

Fig. 5. FTIR spectra of Pt-DD catalyst at room temperature after adsorption of various $^{13}CO/^{12}CO$ mixtures. The spectra shown correspond to 100% ^{12}CO, 78% ^{12}CO, 49% ^{12}CO, 25% ^{12}CO, 13% ^{12}CO, and 0% ^{12}CO.

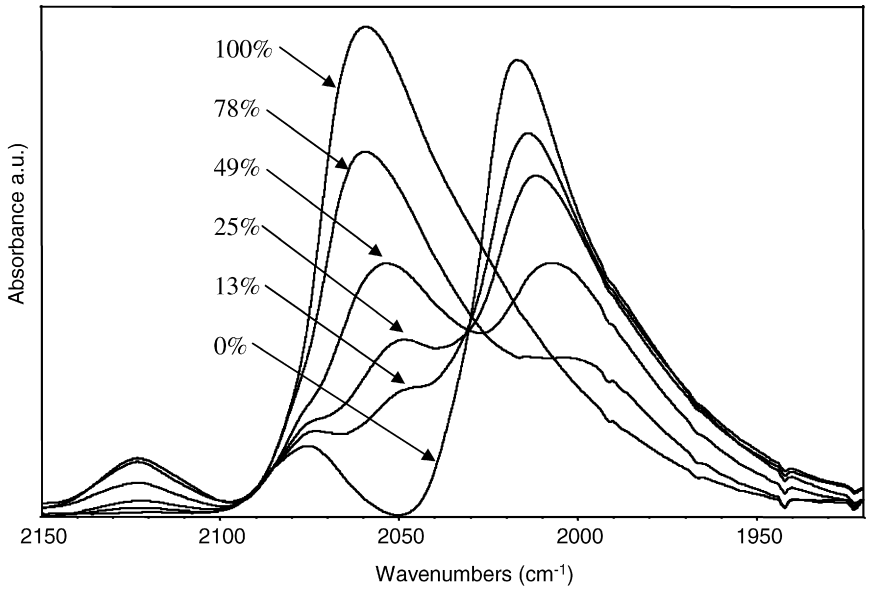

Fig. 6. FTIR spectra of $Pt_{25}Cu_{75}$-DD catalyst at room temperature after adsorption of various $^{13}CO/^{12}CO$ mixtures. The spectra shown correspond to 100% ^{12}CO, 78% ^{12}CO, 49% ^{12}CO, 25% ^{12}CO, 13% ^{12}CO, and 0% ^{12}CO.

with previous reports for supported Pt catalysts [40,47,52]. The linear curve fit of the data from $Pt_{25}Cu_{75}$-DD (squares) suggests a singleton frequency of 2042 ± 2 cm^{-1} for ^{12}CO stretch. The dipole shift in this case is 17 cm^{-1} relative to that of the $Pt_{25}Cu_{75}$-DD catalyst at 100% ^{12}CO. This smaller dipole shift compared with that of the Pt-DD catalyst is due to the addition of Cu, which breaks up Pt ensembles and thus weakens the dipole–dipole interactions that are present.

Although evidence has been reported to show an electronic effect between Cu and Pt [14], based on the foregoing analysis, there appears to be little if any electronic (i.e., chemical) modification of Pt by Cu in the $Pt_{25}Cu_{75}$ catalyst. Although it would be reasonable to expect that Cu might donate electron density to Pt atoms within the alloy or particles, the current results suggest that geometric or structural effects are predominant. This conclusion is consistent with previous studies [48,52], including work by Hoover et al. [34] that explored the structural and catalytic properties of dendrimer-derived Pt–Cu catalysts.

3.3. Hydrodechlorination of 1,2-dichloroethane

In this section, we report results for the reaction rates and selectivity for hydrodechlorination of 1,2-dichloroethane over dendrimer-derived Pt and Pt–Cu catalysts. All kinetic evaluations were done at identical conditions of feed composition, catalyst weight, and flow rates, allowing direct comparison of conversions and selectivities at a given temperature. In the absence of H_2, dechlorination of DCE over the Pt and $Pt_{25}Cu_{75}$ catalysts showed about 300-fold and 30-fold lower reactivity, respectively, compared with that of the hydrodechlorination process at 275 °C. Furthermore, C_2H_4 was the only product observed during dechlorination of DCE. The very small amounts of C_2H_4 formed from decomposition of DCE over Cu catalyst are due to the formation of stable surface C–

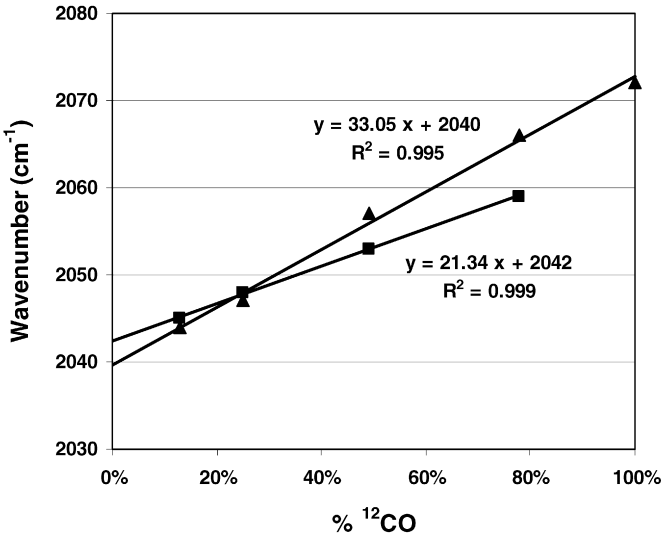

Fig. 7. Infrared frequency of adsorbed ^{12}CO vs. ^{12}CO concentration in the isotope mixture for the Pt (triangles) and $Pt_{25}Cu_{75}$ (squares) catalysts.

Cl species that foul the active Cu sites [53]; therefore, H_2 is needed for high activity and catalyst stability.

3.3.1. Catalyst stability

Fig. 8 shows the changes in conversion and selectivity with time on stream (TOS) at 275 °C for hydrodechlorination of DCE over Cu and $Pt_{25}Cu_{75}$ catalysts, respectively, at identical reaction conditions. For the Cu catalyst (Fig. 8a), slow deactivation was observed over the 16 h run time. Specifically, the initial activity of 77% conversion decreased monotonically to 63%, for a total loss of about 20% of the initial reactivity. In addition, changes in selectivity also were observed for the Cu catalyst; the selectivity toward C_2H_4 decreased from 67% to 37%, whereas that selectivity toward C_2H_6 increased from 33% to 63% over the 16 h runtime. The formation of stable surface Cu–Cl species from C–Cl bond cleavage [54] led to a decrease in available Cu sites, leading to an overall activity decrease. Apparently, the dissociative adsorption of H_2 on surface Cu sites was not as adversely affected on the Cl-poisoned Cu surface as was C–Cl bond dissociation, because hydrogenation to form C_2H_6 became more selective. The observed increase in selectivity toward C_2H_6 suggests that the existence of smaller Cu ensembles

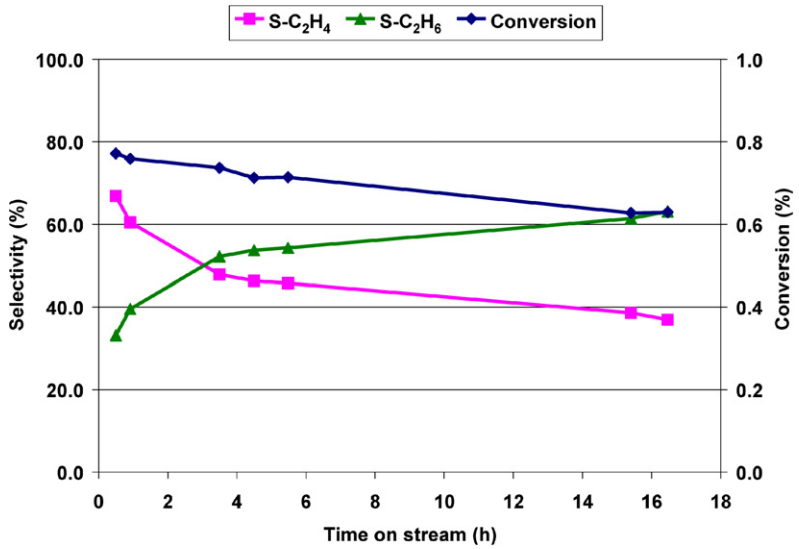

(a)

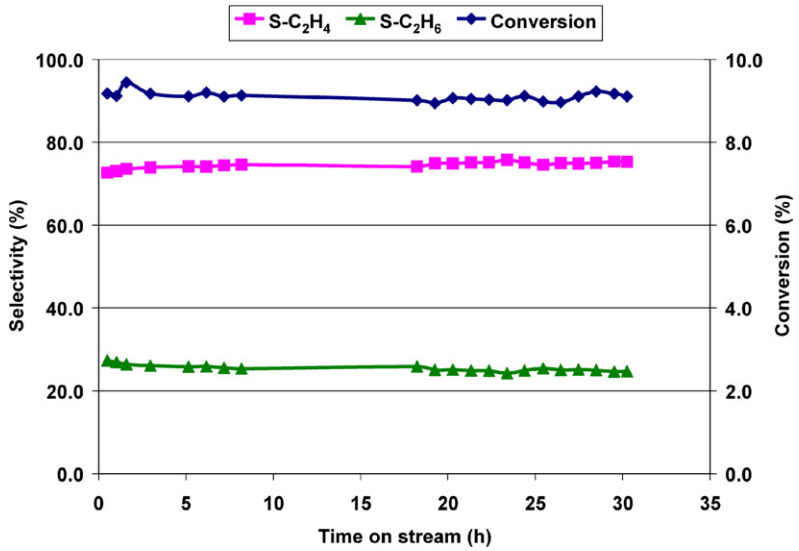

(b)

Fig. 8. Conversion and selectivity as a function of time on stream at 275 °C for the (a) Cu and (b) $Pt_{25}Cu_{75}$ catalysts.

Table 3
Summary of kinetic data for hydrodechlorination of DCE over supported catalysts at steady state (Feed: 1.6% DCE, 16.4% H_2, balance He. Flow rate is 60 SCCM for GHSV = 14900 h^{-1})

Temperature and catalyst	1,2-DCE activity		Selectivity (%)		
	Conversion (%)	TOF (s^{-1})[a]	C_2H_6	C_2H_5Cl	C_2H_4
200 °C					
Pt	4.5	0.02	81.5	18.5	–
$Pt_{50}Cu_{50}$	1.7	0.02	86.9	13.1	–
$Pt_{25}Cu_{75}$	0.8	1.02	74.9	–	25.1
225 °C					
Pt	10.1	0.05	85.5	14.5	–
$Pt_{50}Cu_{50}$	4.0	0.04	89.7	10.3	–
$Pt_{25}Cu_{75}$	2.1	2.71	57.4	–	42.6
250 °C					
Pt	20.7	0.10	89.9	10.1	–
$Pt_{50}Cu_{50}$	8.4	0.09	91.7	8.3	–
$Pt_{25}Cu_{75}$	4.8	6.09	40.7	–	59.3
275 °C					
Pt	41.0	0.19	95.0	5.0	–
$Pt_{50}Cu_{50}$	16.3	0.17	93.4	6.6	–
$Pt_{25}Cu_{75}$	9.7	12.36	29.4	–	70.6
Cu	0.7	n.c.[b]	33.0	–	67.0
300 °C					
Cu	1.5	n.c.	24.8	–	75.2
325 °C					
Cu	3.2	n.c.	16.2	–	83.8

[a] TOF: DCE molecules reacted/(Pt-site s).
[b] n.c. = not calculated; Pt surface area: Pt = 0.755 m^2/g_{cat}, $Pt_{50}Cu_{50}$ = 0.354 m^2/g_{cat}, $Pt_{25}Cu_{75}$ = 0.0028 m^2/g_{cat}.

on the Cl-poisoned surface favors hydrogenation of C_2H_4 to C_2H_6 [18].

In contrast, the $Pt_{25}Cu_{75}$ catalyst showed high activity and stability; no deactivation or change in product distribution was observed over 30 h TOS (Fig. 8b). Stable performance of a similar catalyst of a Pt–Cu catalyst with a Pt:Cu atomic ratio of 1:1 has been reported previously over 30 h TOS [18]. In a Pd–Pt bimetallic catalytic system, Karpinski et al. [23] found that the small amount of Pt doped into Pd showed better resistance against carbiding than monometallic Pd, due to formation of mixed Pd–Pt ensembles that led to enhanced overall activity and selectivity for partial hydrodehalogenation. We discuss the proposed reaction mechanism on $Pt_{25}Cu_{75}$ catalyst later in this paper.

3.3.2. Catalyst kinetic evaluation

Hydrodechlorination of DCE at extended conditions was further investigated for the Pt and $Pt_{50}Cu_{50}$ compositions, as well as for the $Pt_{25}Cu_{75}$ and Cu catalysts at similar reaction conditions (feed composition and space velocity) from 200 °C to 325 °C. Mean values of DCE conversions and selectivities toward C_2H_6, C_2H_4, and C_2H_5Cl for different catalysts are summarized in Table 3. Catalyst activities were expressed in terms of DCE conversion and turnover frequency (TOF) based on surface Pt sites.

As shown in Table 3, all of the Pt-containing catalysts were active for hydrodechlorination of DCE between 200 °C and 275 °C. The Pt and $Pt_{50}Cu_{50}$ catalysts produced mainly C_2H_6, with smaller amounts of C_2H_5Cl. The selectivity patterns were essentially the same for these two catalysts. The selectivity toward C_2H_6 increased from 81.5% to 95% for the Pt catalyst and increased from 86.9% to 93.4% for the $Pt_{50}Cu_{50}$ catalyst as the reaction temperature increased from 200 °C to 275 °C. The similarities between the Pt and $Pt_{50}Cu_{50}$ catalysts in both activity and selectivity suggest that Pt dominated catalyst performance. Thus, the role of Cu in the $Pt_{50}Cu_{50}$ catalyst is not obvious. This is further corroborated by the similar TOFs for both Pt and $Pt_{50}Cu_{50}$ catalysts. Whereas the DCE conversion for the Pt catalyst was about 2.5-fold greater than that of the $Pt_{50}Cu_{50}$ from 200 °C to 275 °C, the TOF values were essentially identical.

Table 4
Apparent activation energies for the formation of various products on different catalysts

Catalysts	Apparent activation energy, E_a (kcal/mol)		
	C_2H_6	C_2H_5Cl	C_2H_4
Pt	16.1	9.3	
$Pt_{50}Cu_{50}$	16.0	10.8	
$Pt_{25}Cu_{75}$	9.3		22.0
Cu[a]	8.6		22.8

[a] Data were obtained by averaging the data collected during the first 2 h of reaction time over the temperature range 275–325 °C.

In contrast, the performance of $Pt_{25}Cu_{75}$ differed markedly from that of the Pt and $Pt_{50}Cu_{50}$ catalysts. The product distribution more closely resembled that of the Cu catalyst, with C_2H_4 and C_2H_6 as the reaction products. Moreover, activity expressed in terms of TOF was 50–70 times that of the Pt and $Pt_{50}Cu_{50}$. Because hydrodechlorination of DCE has been reported to be a structure-insensitive reaction [55], the unusually high TOF value for DCE conversion on the $Pt_{25}Cu_{75}$ catalyst likely is related to the direct participation of neighboring Cu sites in a bifunctional mode of catalytic transformation. Clearly, the selectivity of the $Pt_{25}Cu_{75}$ is closely linked to the surface Cu sites, whereas the much higher activity and stability of the $Pt_{25}Cu_{75}$ composition (Fig. 8) can be attributed to the hydrogenation ability of the Pt sites.

At similar reaction conditions, the Cu catalyst gave very low DCE conversions, with <0.1% conversion observed at temperatures below 250 °C (not shown). Even at higher temperatures, conversion increased only from 0.7% at 275 °C to 3.2% at 325 °C, 1–2 orders of magnitude lower than those of the Pt-containing catalysts. Furthermore, the selectivity toward C_2H_4 increased from about 67% at 275 °C to >80% at 325 °C. The data for the Cu catalyst were obtained by averaging the data collected over 2 h of reaction, because slow deactivation was observed for this catalyst.

In general, the overall activity trend for DCE conversion followed the sequence Pt > $Pt_{50}Cu_{50}$ > $Pt_{25}Cu_{75}$ ≫ Cu. For the Pt and $Pt_{50}Cu_{50}$ catalysts, catalytic activity was related only to the relative amounts of Pt in these catalysts, whereas for the $Pt_{25}Cu_{75}$ catalyst, the activity was related to the existence of a bifunctional bimetallic Pt–Cu catalyst. The bifunctional effects are typically interpreted in terms of alterations in either the electronic structure of the active sites (i.e., electronic effects) or the changes in the geometry of the active metal sites (i.e., ensemble effects) [5,9,12]. Our FTIR studies indicate that Cu did indeed dilute the Pt surface into smaller ensembles of adjacent Pt sites, which would be expected to lower the activity of the $Pt_{50}Cu_{50}$ and $Pt_{25}Cu_{75}$ catalysts on a reactant conversion basis. Therefore, the much higher TOF of the $Pt_{25}Cu_{75}$ catalyst strongly suggests that the dilution effect of Cu was greatly outweighed by the formation of a bifunctional catalyst.

Apparent activation energies for the formation of various products during hydrodechlorination of DCE over the different catalysts are listed in Table 4. The calculations are based on the slopes of Arrhenius plots for different products at differential conversion of DCE over the temperature range 200–275 °C. Table 4 shows that the Pt and $Pt_{50}Cu_{50}$ catalysts had similar activation energies of about 16 and 10 kcal/mol for the formation of C_2H_6 and C_2H_5Cl, respectively. The selectivity trends for the Pt and $Pt_{50}Cu_{50}$ catalysts also were very similar, indicating that the catalytic performance of the latter was due primarily to the Pt component. It has been reported that Ni catalysts modified by low concentrations of Cu were not influenced by the Cu component [56], consistent with this apparent similar effect of the addition of Cu on Pt for the $Pt_{50}Cu_{50}$ catalyst. At a Pt:Cu atomic ratio of 1:1, the surface of $Pt_{50}Cu_{50}$ catalyst apparently was still Pt-enriched. This Pt enrichment can be

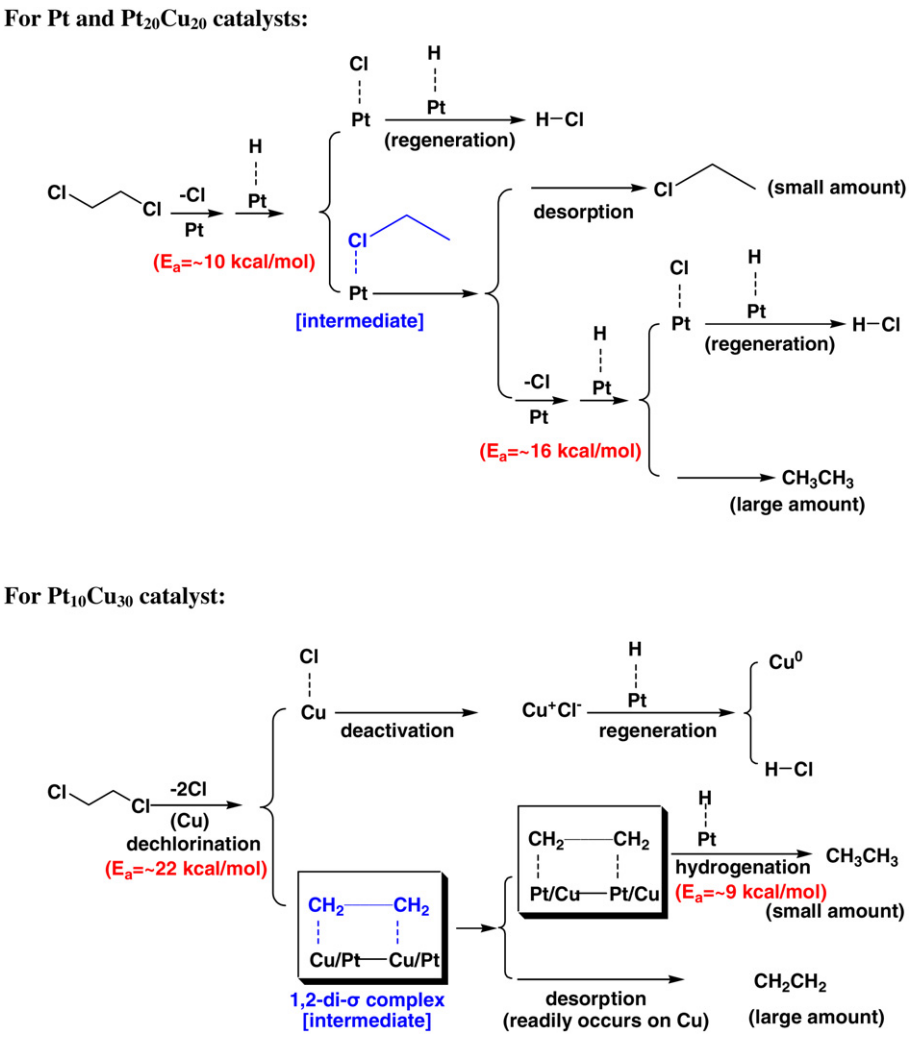

Fig. 9. Proposed reaction schemes for hydrodechlorination of DCE.

further confirmed by the absence of C_2H_4 in the final products, because large Cu ensembles appear to favor the dechlorination of DCE to C_2H_4 [18]. Therefore, for the $Pt_{50}Cu_{50}$ catalyst, the addition of Cu appeared to simply cover the surface Pt sites, thereby decreasing the overall catalytic activity on a reactant conversion basis, but not on a per Pt site basis (i.e., similar TOF values). For the $Pt_{25}Cu_{75}$ catalyst, the activation energies were 9.3 and 22 kcal/mol for the formation of C_2H_6 and C_2H_4, respectively, very similar to those for the Cu catalyst. The similar selectivity trends for the $Pt_{25}Cu_{75}$ and Cu catalysts at 275 °C (cf. Table 3) confirm the important role of Cu in the former.

These results from both the activation energy and selectivity analyses suggest the formation of two different types of Pt–Cu bimetallic catalysts, a Cu-diluted Pt catalyst ($Pt_{50}Cu_{50}$) with similar kinetic behavior as the Pt catalyst, and a Cu-enriched Pt catalyst ($Pt_{25}Cu_{75}$) that more closely resembles the Cu catalyst in terms of production distribution and reaction energetics. The much greater activity and more stable behavior of the $Pt_{25}Cu_{75}$ catalyst indicate the strong roles of both the Cu and Pt components in this case, however.

3.3.3. *Catalytic reaction mechanism analysis*

For hydrodechlorination of DCE to occur, both DCE and H_2 must be adsorbed to facilitate both C–Cl and H–H dissociation on the catalyst surface. Hydrogen is dissociatively adsorbed on most transition metals; for example, the heat of H_2 adsorption is about 9 kcal/mol on Cu(110) surfaces and 13 kcal/mol on Pt(110) surfaces. The activation energy for H_2 dissociation is negligible on Pt(110) and is only 1–2 kcal/mol on Pt(111). For Cu surfaces, the activation energies are about 10 kcal/mol on both Cu(110) and Cu(111) surfaces [29]. Thus, although the heats of adsorption are only 4 kcal/mol different for Pt(110) and Cu(110), there is a 10-kcal/mol energy difference for the activation energies of dissociation, which has been attributed to the differences in the d-band electron densities of Pt and Cu. Consequently, H_2 dissociates readily on Pt surfaces, whereas dissociation of H_2 on Cu is an activated process [57]. Proposed reaction schemes for the hydrodechlorination of DCE on the catalysts evaluated in the present study are shown in Fig. 9.

Several different mechanisms for the hydrodechlorination of DCE have been reported. d'Itri [16,18] and Lambert et al. [4] have proposed homolytic C–Cl bond scission on Pt and Pd sites, followed by hydrogenation of the surface alkyl fragment to form C_2H_6. Bozzelli et al. [58] have proposed successive C–Cl bond scission over Rh catalysts, where C_2H_5Cl is first formed from the reaction of dichloroethane with H_2. The intermediate C_2H_5Cl can be hydrodechlorinated to form C_2H_6. Heinrichs et al. [19] proposed a model based on the Langmuir–Hinshelwood mechanism involving two types of different sites, which corresponds to a mechanism involving dechlorination of DCE into C_2H_4 occurring on Ag through dissociative adsorption with successive breaking of the two C–Cl bonds and desorption of C_2H_4. Campbell et al. [59] have investi-

gated the hydrogenolysis of C_2H_5Cl over polycrystalline Pt films at 100–206 °C and found that Pt caused C_2H_5Cl to decompose by the following reaction: $C_2H_5Cl + H_2 \rightarrow C_2H_6 + HCl$. In addition, the activation energy was found to be 12 kcal/mol, a value between the activation energies of 10 and 16 kcal/mol for the formation of C_2H_5Cl and C_2H_6, respectively, over Pt and $Pt_{50}Cu_{50}$ found in the present study.

For Cu-rich catalysts such as $Pt_{25}Cu_{75}$ and Cu, the situation is quite different; C–Cl bond cleavage occurs readily on the Cu surface to form strong Cu–Cl bonds [54]. For example, hydrogenolysis of CH_3Cl over Cu has been reported to form strong Cu–Cl bonds, indicating the potential poisoning of a Cu surface by Cu–Cl species [56]. Because Cu is a poor hydrogenation catalyst, the formation of HCl to regenerate the Cu surface is limited; however, the existence of adjacent Pt sites as in the $Pt_{25}Cu_{75}$ bimetallic catalyst permits the facile adsorption of H_2, which provides an abundant source of adsorbed H to effectively remove strongly bonded Cl on adjacent Cu sites through the formation of HCl.

The activation energies of 22.0 and 9.3 kcal/mol for the formation of C_2H_4 and C_2H_6, respectively, on $Pt_{25}Cu_{75}$ catalysts agree well with the activation energies of 10.8 kcal/mol for the hydrogenation of C_2H_4 on Pt(111) surfaces reported by Grunes et al. [60] and 21 kcal/mol for dissociation of DCE over polycrystalline Cu surfaces reported by Walter et al. [61]. For the Cu-catalyzed dechlorination of DCE to form C_2H_4, Cu–Cl species are formed on the Cu surface by dechlorination before removal as HCl by reaction with adsorbed H on the Cu surface. The relatively low rate of dissociative H_2 adsorption limits the rate of reaction of DCE. The dissociation of both C–Cl bonds in DCE appears to occur in the same adsorption step, because no C_2H_5Cl is formed as a reaction product. Thus, Cu ensembles containing a critical number of adjacent Cu sites are likely required for both C–Cl bond dissociation to occur in the same surface reaction step to form two Cu–Cl species and a di-σ-adsorbed $\cdot CH_2–CH_2\cdot$ species. In the absence of Pt sites (as in Cu), there must be vacant Cu sites capable of the dissociative adsorption of H_2 to remove the surface Cu–Cl species as HCl.

For the $Pt_{25}Cu_{75}$ bimetallic catalyst, some of the adsorbed Cu-bound $\cdot CH_2–CH_2\cdot$ species can undergo rapid hydrogenation by H adsorbed on adjacent Pt sites to form C_2H_6 as the reaction product. Again, the failure to observe C_2H_5Cl as a reaction product for $Pt_{25}Cu_{75}$ indicates that desorption of the final product did not occur until saturation to C_2H_6 was complete. Furthermore, because of the presence of adjacent Pt–H species, removal of Cl absorbed on Cu occurred more readily, making the Cu surface active for another catalytic turnover. In this sense, the $Pt_{25}Cu_{75}$ catalyst acted as a bifunctional catalyst, whereby the dechlorination of DCE on Cu ensembles to form the di-$\sigma\cdot CH_2–CH_2\cdot$ intermediate was followed by the hydrogenation of the $\cdot CH_2–CH_2\cdot$ intermediate to form C_2H_6.

4. Conclusion

In this study, a series of SiO_2-supported catalysts were prepared by two different methods, dendrimer G4OH-metal complexes (DD) and the conventional wet co-impregnation of metal salt precursors (CD). The sizes of the Pt and Pt–Cu nanoparticles in these catalysts indicate a smaller average particle size and narrower size distribution for the metal nanoparticles in the DD catalysts than in the CD catalysts. STEM analysis suggests that the G4OH dendrimer was capable of exerting significant control over particle formation and sintering on the catalyst support. FTIR spectroscopy was used to further characterize the adsorption and desorption of CO on these dendrimer-derived catalysts. Differences observed in the IR spectra can be related to differences in the oxidation state, particle size, and relative Pt/Cu composition of the catalysts. The addition of Cu to Pt lowered the stretching frequency for linearly adsorbed CO. Isotope dilution experiment experiments with Pt and $Pt_{25}Cu_{75}$ catalysts showed a singleton frequency of the linearly adsorbed CO on Pt at ca. 2040 cm^{-1} and a dipole–dipole shift of ca. 32 and 17 cm^{-1} for the main band for the Pt and $Pt_{25}Cu_{75}$ catalysts, respectively; however, the similarity in the singleton frequencies suggests little to no electronic modification of the Pt sites by Cu in the $Pt_{25}Cu_{75}$ catalyst.

Different catalytic activity and product selectivity patterns for hydrodechlorination of DCE were observed for these catalysts. Slow deactivation was observed for hydrodechlorination of 1,2-dichloroethane over monometallic Cu catalyst, which showed an activity about one to two orders of magnitude lower than that of the Pt-containing catalysts. The overall activity decreased with increasing Cu loading in the catalysts. The Pt and $Pt_{50}Cu_{50}$ catalysts exhibited the same selectivity patterns, with C_2H_6 as the main product and C_2H_5Cl as a byproduct. On the other hand, C_2H_4 was produced over $Pt_{25}Cu_{75}$ catalyst with selectivity ranging from 25% to 70% depending on the reaction temperature. The $Pt_{50}Cu_{50}$ catalyst has a Pt-enriched surface, whereas the $Pt_{25}Cu_{75}$ has a Cu-enriched surface, which contributes to the difference in selectivity patterns. Activity based on surface Pt sites suggests the formation of a true bimetallic $Pt_{25}Cu_{75}$ catalyst, with bi-functional surfaces favoring the C–Cl bond scission on Cu sites and $\cdot CH_2CH_2\cdot$ intermediate hydrogenation on Pt sites, respectively.

Acknowledgments

This work was supported by a grant from the National Science Foundation (CTS-0103135). The STEM work was sponsored by the Assistant Secretary for Energy Efficiency and Renewable Energy, Office of FreedomCAR and Vehicle Technologies, as part of the High-Temperature Materials Laboratory User Program at Oak Ridge National Laboratory, managed by UT-Battelle for the U.S. Dept. of Energy under contract DE-AC05-00OR22725. The XRD work was performed at Oak Ridge National Laboratory's Center for Nanophase Materials Sciences and was sponsored by the Scientific User Facilities Division, Office of Basic Energy Sciences, U.S. Department of Energy.

Supplementary information

Supplementary material associated with this article can be found, in the online version, at doi: 10.1016/j.jcat.2008.07.018.

References

[1] S. Imamura, K. Takai, T. Yamate, K. Utani, J. Jpn. Pet. Inst. 46 (2003) 138–141.
[2] L.E. Manzer, P.R. Resnick, Process for the preparation of halogenated 2,2-bis-(trifluoromethyl)-1,3-dioxolanes, du Pont de Nemours, E.I. and Co., USA. Application: WO, 1991, 38 pp.
[3] B. Coq, G. Ferrat, F. Figueras, J. Catal. 101 (1986) 434–445.
[4] S. Lambert, F. Ferauche, A. Brasseur, J.-P. Pirard, B. Heinrichs, Catal. Today 100 (2005) 283–289.
[5] J.H. Sinfelt, Acc. Chem. Res. 10 (1977) 15–20.
[6] J.H. Sinfelt, Bimetallic Catalysts: Discoveries, Concepts, and Applications, Wiley, New York, 1983.
[7] C.T. Campbell, Annu. Rev. Phys. Chem. 41 (1990) 775–837.
[8] J.A. Rodriguez, D.W. Goodman, J. Phys. Chem. 95 (1991) 4196–4206.
[9] L. Guczi, Catal. Today 101 (2005) 53–64.
[10] V. Ponec, Catal. Today 10 (1991) 251–258.
[11] V.D. Stytsenko, Appl. Catal. A Gen. 126 (1995) 1–26.
[12] J.A. Rodriguez, Surf. Sci. Rep. 24 (1996) 223–287.
[13] N. Toshima, T. Yonezawa, New J. Chem. 22 (1998) 1179–1201.
[14] L. Melo, D. Velasquez, A. Llanos, L. Garcia, G. Giannetto, M. Guisnet, P. Magnoux, F. Alvarez, Catal. Lett. 78 (2002) 57–63.
[15] W.D. Rhodes, J.L. Margitfalvi, I. Borbath, K. Lazar, V.I. Kovalchuk, J.L. d'Itri, J. Catal. 230 (2005) 86–97.
[16] L.S. Vadlamannati, V.I. Kovalchuk, J.L. d'Itri, Catal. Lett. 58 (1999) 173–178.

[17] L.S. Vadlamannati, D.R. Luebke, V.I. Kovalchuk, J.L. d'Itri, Stud. Surf. Sci. Catal. A 130 (2000) 233–238.
[18] V.Y. Borovkov, D.R. Luebke, V.I. Kovalchuk, J.L. d'Itri, J. Phys. Chem. B 107 (2003) 5568–5574.
[19] B. Heinrichs, J.-P. Schoebrechts, J.-P. Pirard, J. Catal. 200 (2001) 309–320.
[20] B. Heinrichs, F. Noville, J.-P. Schoebrechts, J.-P. Pirard, J. Catal. 220 (2003) 215–225.
[21] B. Heinrichs, F. Noville, J.-P. Schoebrechts, J.-P. Pirard, J. Catal. 192 (2000) 108–118.
[22] B. Heinrichs, P. Delhez, J.-P. Schoebrechts, J.-P. Pirard, J. Catal. 172 (1997) 322–335.
[23] M. Legawiec-Jarzyna, A. Srebowata, W. Juszczyk, Z. Karpinski, Appl. Catal. A Gen. 271 (2004) 61–68.
[24] L.N.M. Ito (MI), M.E. Jones (Midland, MI), S.R. Bare (Midland, MI), Preparation of bimetallic catalysts for hydrodechlorination of chlorinated hydrocarbons, The Dow Chemical Company, Midland, MI, US (1997).
[25] P.H. Delhez (BE), B. Heinrichs (Liege, BE), J.-P. Pirard (Chenee, BE), J.-P. Schoebrechts (Grez-Doiceau, BE), Process for the preparation of a catalyst and its use for the conversion of chloroalkanes into alkenes containing less chlorine, Solvay (Societe Anonyme), Brussels, BE, US (2000).
[26] I. Bönicke, W. Kirstein, S. Spinzig, F. Thieme, Surf. Sci. 313 (1994) 231–238.
[27] J.K. Eve, E.M. McCash, Chem. Phys. Lett. 313 (1999) 575–581.
[28] C.J. Zhang, R.J. Baxter, P. Hu, A. Alavi, M.H. Lee, J. Chem. Phys. 115 (2001) 5272–5277.
[29] L. Xiong, A. Manthiram, J. Electrochem. Soc. 152 (2005) A697–A703.
[30] S. Koh, P. Strasser, J. Am. Chem. Soc. 129 (2007) 12624–12625.
[31] D.V. Pugh, A. Dursun, S.G. Corcoran, J. Mater. Res. 18 (2003) 216–221.
[32] T.H. Mourey, S.R. Turner, M. Rubinstein, J.M.J. Frechet, C.J. Hawker, K.L. Wooley, Macromolecules 25 (1992) 2401–2406.
[33] A.W. Bosman, H.M. Janssen, E.W. Meijer, Chem. Rev. (Washington, D.C.) 99 (1999) 1665–1688.
[34] D.A. Tomalia, H. Baker, J. Dewald, M. Hall, G. Kallos, S. Martin, J. Roeck, J. Ryder, P. Smith, Polym. J. (Tokyo, Japan) 17 (1985) 117–132.
[35] H. Xie, Y. Gu, H.J. Ploehn, Nanotechnology 16 (2005) 492–501.
[36] Y. Gu, H. Xie, J. Gao, D. Liu, C.T. Williams, C.J. Murphy, H.J. Ploehn, Langmuir 21 (2005) 3122–3131.
[37] R.M. Crooks, M. Zhao, L. Sun, V. Chechik, L.K. Yeung, Acc. Chem. Res. 34 (2001) 181–190.
[38] H. Xie, H.J. Ploehn, C.T. Williams, Synthesis and characterization of dendrimer-derived Pt-Cu/SiO_2 catalysts (2008), in preparation.
[39] D.S. Deutsch, G. Lafaye, D. Liu, B. Chandler, C.T. Williams, M.D. Amiridis, Catal. Lett. 97 (2004) 139–143.
[40] P. Hollins, Surf. Sci. Rep. 16 (1992) 51–94.
[41] C. De La Cruz, N. Sheppard, Spectrochim. Acta, Part A Mol. Biomol. Spectr. A 50 (1994) 271–285.
[42] P.T. Fanson, W.N. Delgass, J. Lauterbach, J. Catal. 204 (2001) 35–52.
[43] R.K. Brandt, M.R. Hughes, L.P. Bourget, K. Truszkowska, R.G. Greenler, Surf. Sci. 286 (1993) 15–25.
[44] J. Rasko, J. Catal. 217 (2003) 478–486.
[45] S.C. Chang, M.J. Weaver, J. Phys. Chem. 95 (1991) 5391–5400.
[46] C. De la Cruz, N. Sheppard, J. Mol. Struct. 224 (1990) 141–146.
[47] B.D. Chandler, L.H. Pignolet, Catal. Today 65 (2001) 39–50.
[48] R.K. Herz, E.J. Shinouskis, Appl. Surf. Sci. (1977–1985) 19 (1984) 373–397.
[49] M.H. Kim, J.R. Ebner, R.M. Friedman, M.A. Vannice, J. Catal. 208 (2002) 381–392.
[50] A. Dandekar, M.A. Vannice, J. Catal. 178 (1998) 621–639.
[51] J. Lauterbach, R.W. Boyle, M. Schick, W.J. Mitchell, B. Meng, W.H. Weinberg, Surf. Sci. 350 (1996) 32–44.
[52] F.J.C.M. Toolenaar, F. Stoop, V. Ponec, J. Catal. 82 (1983) 1–12.
[53] M. Legawiec-Jarzyna, A. Srebowata, W. Juszczyk, Z. Karpinski, J. Mol. Catal. A Chem. 224 (2004) 171–177.
[54] M.X. Yang, S. Sarkar, B.E. Bent, S.R. Bare, M.T. Holbrook, Langmuir 13 (1997) 229–242.
[55] S. Lambert, C. Cellier, P. Grange, J.-P. Pirard, B. Heinrichs, J. Catal. 221 (2004) 335–346.
[56] Y.H. Choi, W.Y. Lee, Catal. Lett. 67 (2000) 155–161.
[57] R.I. Masel, Principles of Adsorption and Reaction on Solid Surfaces, Wiley, New York, 1995, 848 pp. (approx).
[58] J.W. Bozzelli, Y.-M. Chen, Chem. Eng. Commun. 115 (1992) 1–11.
[59] J.S. Campbell, C. Kemball, Trans. Faraday Soc. 57 (1961) 809–820.
[60] J. Grunes, J. Zhu, M. Yang, G.A. Somorjai, Catal. Lett. 86 (2003) 157–161.
[61] W.K. Walter, R.G. Jones, Surf. Sci. 264 (1992) 391–405.